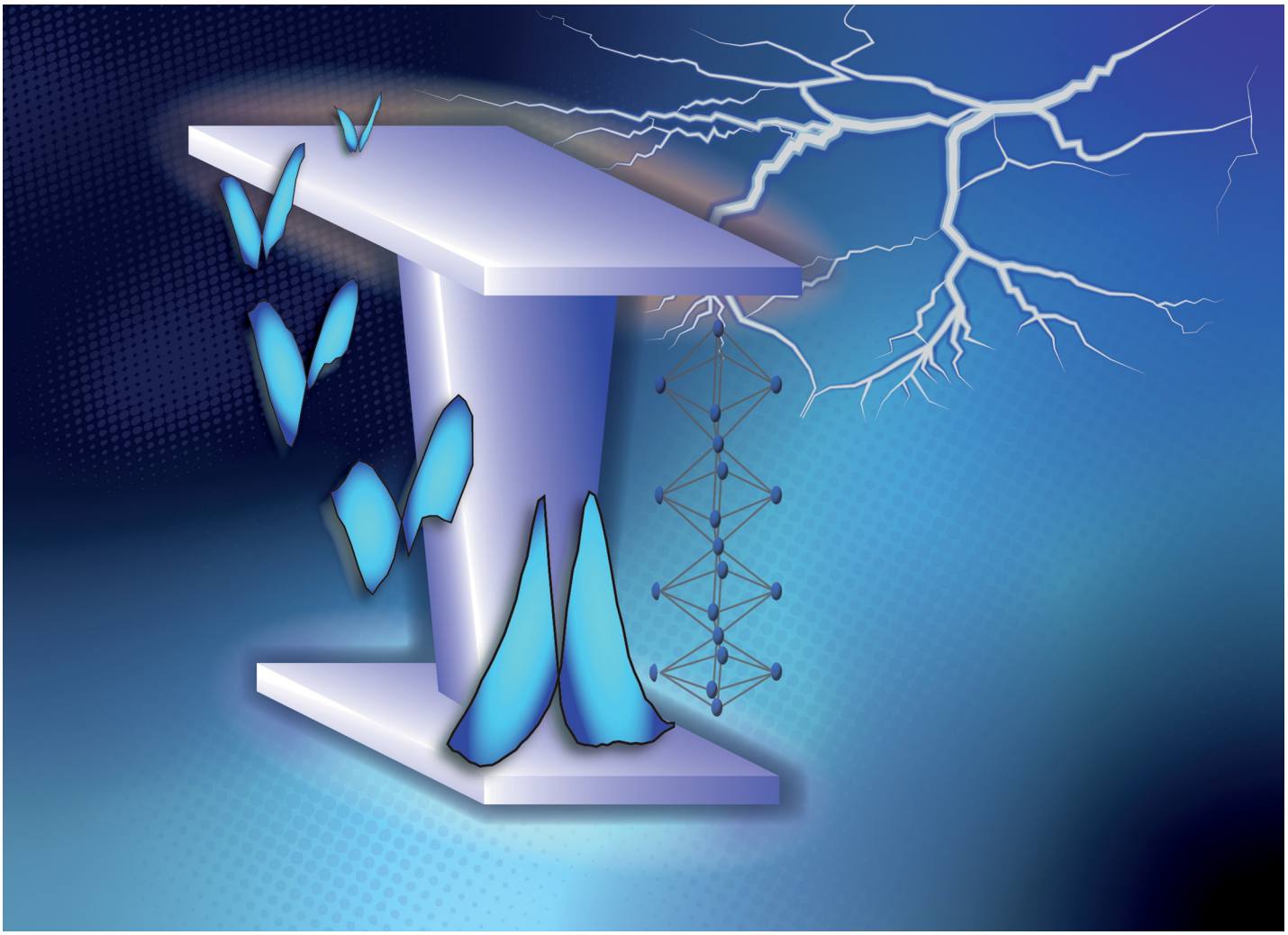

From the Thermal Materials Lab at The Ohio State University, Columbus, Ohio, under the direction of Professor Joseph Heremans.

Electric field-dependent thermal conductivity of relaxor ferroelectric PMN-33PT through changes in the phonon spectrum

This study demonstrates how the thermal conductivity of the relaxor ferroelectric PMN–33PT can be modulated by an electric field through shifts in the phonon spectrum. The work confirms a predictive theory initially developed for PZT, revealing an effect up to two orders of magnitude larger in PMN–33PT. These findings enable progress toward voltage-controlled, all-solid-state heat switches.

Image reproduced by permission of Joseph Heremans from *Mater. Horiz.*, 2025, **12**, 3341.

Image created by Renée L. Ripley.

As featured in:

See Brandi L. Wooten, Joseph P. Heremans *et al.*, *Mater. Horiz.*, 2025, **12**, 3341.

ROYAL SOCIETY OF CHEMISTRY

rsc.li/materials-horizons

Registered charity number: 207890

Materials Horizons

ROYAL SOCIETY OF CHEMISTRY

COMMUNICATION

View Article Online
View Journal | View Issue

Cite this: *Mater. Horiz.*, 2025, 12, 3341

Received 16th December 2024,
Accepted 12th March 2025

DOI: 10.1039/d4mh01845a

rsc.li/materials-horizons

Electric field-dependent thermal conductivity of relaxor ferroelectric PMN-33PT through changes in the phonon spectrum†

Delaram Rashadfar, [a] Brandi L. Wooten *[b] and Joseph P. Heremans *[abc]

In ferroelectric materials, an electric field has been shown to change the phonon dispersion sufficiently to alter the lattice thermal conductivity, opening the possibility that a heat gradient could drive a polarization flux, and technologically, also opening a pathway towards voltage-driven, all solid-state heat switching. In this report, we confirm the validity of the theory originally developed for Pb(Zr,Ti)O_3 (PZT) on the ferroelectric relaxor 0.67Pb[$Mg_{1/3}Nb_{2/3}$]O_3–0.33$PbTiO_3$ (PMN–33PT). In theory, the change in sound velocity and thermal conductivity with an electric field relates to the piezoelectric coefficients and the Grüneisen parameter. It predicts that in PMN–33PT the effect should be an order of magnitude larger and of opposite sign as in PZT; this is confirmed here experimentally. The effects are measured on samples never poled before and on samples that underwent multiple field sweep cycles and passed through two phase transitions with change in temperature. The thermal conductivity changes are linked to variations in the piezoelectric coefficients and can be as large as 8–11% at $T \geq 300$ K. To date, this has been the only means of heat conduction modulation that utilizes changes in the phonon spectrum. While this technology is in its infancy, it offers another path to future active thermal conduction control.

New concepts

This is the second experimental paper in the new field of polarization caloritronics describing the transport of the thermal fluctuations (labeled ferrons) of the polarization responsible for the decrease of the polarization with temperature in ferroelectrics. Ferrons are a subset of phonons that involve the motion of atoms whose charges are responsible for the polarization in ferroelectrics; they are optical phonons strain-coupled to acoustic phonons. They carry heat and polarization fluxes much like magnons do in ferromagnets. The present article reports the electric field dependence of the thermal conductivity of a relaxor ferroelectric, PMN–PT. It shows how a theory developed for ferron transport in PZT applies equally to the relaxor ferroelectric PMN–PT. The novelty and importance of the present paper are that it shows the theory to be predictive: PMN–PT was selected to maximize the effect, which proved indeed up to 2 orders of magnitude larger than in PZT. This is a new approach to the realization of electrically driven all-solid-state heat switches, based on electric-field driven modifications of the phonon spectrum in ferroelectrics. Furthermore, polarization fluxes could potentially lead to a cornucopia of new applications of voltage-driven phenomena including thermal transistors, new thermoelectric concepts, and phonon-based logic and memory devices.

Introduction

Long-range order occurs in materials that are ferromagnetic (FM) or ferroelectric (FE). The interactions between atomic magnetic or electric dipoles lead to a collective magnetization or polarization (M/P) moment that exhibits a hysteresis loop in response to a magnetic or electric field (H/E). At higher fields, dipole moments align with the field direction, achieving saturation at moments (M_S/P_S). At intermediate field strengths, the materials create domains where M/P are oriented in various directions. As the temperature rises, M_S/P_S diminish due to increased thermal fluctuations. Additionally, there exists a non-zero pyroelectric coefficient $\Pi_{PY} \equiv \frac{d|P|}{dT}$ at all field strengths. Both factors indicate that a temperature gradient (∇T) produces a polarization gradient. In irreversible thermodynamics, the changes in extensive quantities such as heat (Q) and magnetization or polarization are linked to a heat flux j_Q accompanied by a spin flux j_S in ferromagnets, and its extension to ferroelectrics the polarization flux j_P, allowing for the expression of polarization Onsager relations:[1]

$$-j_P = \sigma\nabla E - S\sigma\nabla T \quad (1)$$

$$-j_Q = \sigma\Pi\nabla E - \kappa\nabla T \quad (2)$$

where σ is the polarization conductivity tensor, and S, Π, and κ represent the polarization Seebeck, Peltier, and thermal conductivity tensors, respectively.

[a] Department of Mechanical and Aerospace Engineering, Ohio State University, Columbus, OH, 43210, USA. E-mail: brandi.l.wooten.civ@army.mil
[b] Department of Materials Science and Engineering, Ohio State University, Columbus, OH, 43210, USA
[c] Department of Physics, Ohio State University, Columbus, OH, 43210, USA

† Electronic supplementary information (ESI) available. See DOI: https://doi.org/10.1039/d4mh01845a

For FMs, the thermal fluctuations of magnetization involve spin waves or magnons, while in FEs, it relates to a specific type of phonon called ferrons, as identified by Bauer *et al.*[1] Like how M_S decreases with rising temperature due to an increase in magnon population, P_S follows suit due to a higher density of ferrons. Intuitively, in displacement ferroelectrics, ferrons include optical phonons that involve the displacement of the ions that give rise to atomic dipoles. However, the distinction between acoustic and optical modes remains well-defined only at zero wavevector (k); at non-zero k, the optical and acoustic phonons couple due to strain. Ferrons are thus optical and acoustic modes strain-coupled by the piezoelectric coefficients. In principle, one then expects an electric field dependence of the phonon dispersion and hence the lattice thermal conductivity. The former effect is observed in $0.70Pb[Mg_{1/3}Nb_{2/3}]O_3$–$0.30PbTiO_3$ (PMN–30PT)[2] and the latter in $Pb(Zr,Ti)O_3$ (PZT)[3] where the field is shown to affect the lattice thermal conductivity by about 2%. The present article strongly amplifies the earlier work of Wooten *et al.*[3] by showing effects one and two orders of magnitude larger in the field-dependent thermal conductivity of PMN–33PT.

A quantitative theory[3] for the dependence of sound velocity, lattice thermal conductivity and diffusivity with no adjustable parameters relates changes in the sound velocity v to the piezoelectric coefficients d_{33} and d_{31} and the Grüneisen parameter γ. Fundamentally, the theory is based on the change of the phonon dispersions with the change in the volume of the sample, which is characterized by the Grüneisen parameter. The applied electric field then changes the volume of the sample as characterized by the piezoelectric coefficients. Putting both together will then predict the change in sound velocity and thus in the lattice thermal conductivity. Quantitatively, piezoelectric coefficients are defined as $d_{33} = \frac{\partial e_{33}}{\partial E}$ and $d_{31} = \frac{\partial e_{11}}{\partial E}$, where $e_{33(11)}$ is the strain tensor component that gives the compression or expansion along (perpendicular to) the direction of ferroelectric order, which is parallel to the applied field $E = E_3$. The mode (i) and wavevector (k)-dependent Grüneisen parameter is the logarithmic derivative of that phonon mode's frequency *vis-à-vis* the volume V of the sample, $\gamma(i,k) \equiv \frac{\mathrm{d}\ln(\omega(i,k))}{\mathrm{d}\ln(V)}$, by definition. For longitudinal or transverse acoustic phonons at low k (i = LA or TA, respectively), $\gamma(i) \equiv \frac{\mathrm{d}\ln(v(i))}{\mathrm{d}\ln(V)}$. The basis of the theory is to first describe how the piezoelectric coefficients relate the change in volume of the sample with the applied field to ($d_{33} + 2d_{31}$) and then relate that to the logarithmic derivative of the sound velocity for each mode:

$$\frac{v'}{v_0} = \frac{\mathrm{d}\ln(v)}{\mathrm{d}E} = -\gamma(d_{33} + 2d_{31}). \quad (3)$$

Here, $v' = \frac{\mathrm{d}v}{\mathrm{d}E}$ is the derivative of the sound velocity with respect to the applied electric field and γ is the specific heat-weighted mode and wavevector average of $\gamma(i,k)$. From the sound velocity we move to the thermal conductivity using the equation $\kappa = \frac{1}{3}Cvl = \frac{1}{3}Cv^2\tau$, where C represents the volumetric specific heat, l the mean free path, and τ the relaxation time; here, v is the average velocity of the LA and 2 TA modes. At temperatures above the Debye temperature (Θ_D ~150–180 K for PMN–PT[4]; this is the Debye temperature for the monoclinic (M) phase, and since the differences between the M_A and M_C phases are only in the direction of the polarization vector, no significant difference is expected), the specific heat is constant with E being a function of only the number of atoms per unit volume n, $C = 3nk_B$ (k_B is the Boltzmann constant).

In a first approximation, above 200 K, we hypothesize that the scattering time is unaffected by the electric field, based on temperature-dependent measurements by Mante and Folger on $BaTiO_3$.[5] There, below 10 K, the phonon mean free path is on the order of the domain size and since this property is field sensitive, the thermal conductivity also depends on the electric field. This effect vanishes at higher temperatures where phonon–phonon scattering dominates. Assuming that the relaxation time is independent of the electric field ($T \gg 10$ K), we can relate the electric field dependency of both the sound velocity and thermal conductivity κ above the Debye temperature as:

$$\frac{\kappa'}{\kappa_0} = 2\frac{v'}{v_0} \quad (4)$$

where again $\kappa' = \frac{\mathrm{d}\kappa}{\mathrm{d}E}$. The validity of eqn (3) and (4) was tested experimentally on PZT and confirmed by Wooten *et al.*[3] without the use of adjustable parameters since d_{33}, d_{31}, and γ were known.

While this approximation holds well for PZT,[3] it is more questionable for PMN–PT. Indeed, neutron scattering data on PMN-30PT[2] show both strong softening of the lower section of the TA phonon branch and a marked decrease in phonon lifetime. In this case,

$$\frac{\kappa'}{\kappa_0} = 2\frac{v'}{v_0} + \frac{\tau'}{\tau}. \quad (5)$$

where $\tau' = \mathrm{d}\tau/\mathrm{d}E$. The latter term is not attributed to domain wall scattering, but rather to the change in phase space for acoustic phonons to scatter due to changes in the phonon spectrum with an electric field. In that sense, the second term in eqn (5) is also due to changes in the phonon spectrum. Experimentally, comparing dynamic measurements of the sound velocity and the thermal conductivity changes with the field provides a test for the validity of eqn (4).

If eqn (3) and (4) have predictive values, they allow us to sort amongst known ferroelectrics for the compound that has the largest field dependence of thermal conductivity and is thus most useful in thermal switching applications. The primary application for modulating the heat conduction in FE materials lies in the implementation of voltage-driven heat switches. Heat switches, or thermal transistors, are a particularly useful element in heat management,[6] which is key to the continued scaling up of the complexity in advanced semiconductor integrated circuits. They are also the key elements in all-solid-state

power generation and refrigeration cycles based on electrocaloric and magnetocaloric effects, where no fluid is circulated but only heat. Many heat switching technologies exist,[7] including one that is based on domain wall motion in ferroelectrics[8] and another on the electrophononic effect based on the lowering of symmetry in ferroelectrics;[9–11] however, the mechanism exploited here, the phonon spectrum shifts *via* an electric field, promises to give reasonable effects over a large temperature range if maximized. Ultimately, the goal is to create an electrically modulated, voltage-driven thermal switch with the largest switching ratio.

Eqn (3) sheds light on the material parameters needed to maximize the thermal modulation – very anharmonic phonons denoted by a large Grüneisen parameter γ and maximization of the summation $(d_{33} + 2d_{31})$. The relaxor ferroelectric solid solution system $Pb[Mg_{1/3}Nb_{2/3}]O_3$–$PbTiO_3$ (PMN–PT) is known to exhibit enhanced piezoelectricity. In this work, we investigate the thermal conductivity modulation of PMN–PT using an electric field with the specific composition of $(1 - x)Pb[Mg_{1/3}Nb_{2/3}]O_3$–$xPbTiO_3$ with x estimated to be between 0.3 and 0.33 (further abbreviated as PMN–33PT throughout the text). The main practical and commercial advantages of PMN–PT over PZT are its much larger piezoelectric coefficient. This is the reason we picked it for this study, since our theory predicted that this should lead to a much stronger dependence of the thermal conductivity on the electric field. In the uncycled sample, we prove this is indeed the case, and the theory is followed quantitatively. To our surprise, this sensitivity increases further to 10% in the cycled material. Our model did not predict that, and we will discuss its possible origin. The disadvantage of PMN–PT is the fact that it undergoes various phase transitions with temperature and an applied electric field, which complicated the sample-to-sample reproducibility of the properties of the cycled samples, a difficulty already described by the wide variation in the reported values of d_{33} of commercially cycled PMN–33PT (d_{33} ranging from 1300 to 2500 pC/N in the literature).

Methods

Materials procurement & preparation

Single-crystals of PMN-xPT ($0.3 \leq x \leq 0.33$) with a poling direction of (001) and a thickness of 0.5 mm were obtained from MSE Supplies. To apply an electric field, 10 nm of Ti and then 90 nm of Au were evaporated onto the primary surfaces in a CHA solution system E-gun evaporator.

Sound velocity

To measure the sound velocity, a fresh sample of PMN–33PT with evaporated gold was cleaved into a parallelopiped of approximate size 3 mm × 1 mm. Coiled Cu wires (Omega, diameter of 25 μm) were attached to the electrodes to apply an electric field. DC voltage was applied using a Stanford Research Systems' Data Precision 8200. The sample was placed in a resonant ultrasound spectrometer (RUS) (Alamo Creek Engineering). In the RUS, the sample was subjected to ultrasound frequencies that were amplified if they corresponded to a natural resonant frequency of the entire sample. The peak corresponding to the longitudinal frequency of the compressive wave in the whole sample was selected. This targeted longitudinal resonant frequency was calculated using the detailed sample geometry and dimensions, the Young's modulus, the density provided from the manufacturer's website. The shift of the peak frequency, f, with an applied voltage was tracked by hand.

Thermal conductivity

Thermal conductivity measurements were conducted using the static heater-and-sink method on two PMN–33PT samples. Two type T thermocouples consisting of a copper and Constantan wire were adhered to the first PMN–33PT sample using GE Varnish, which is thermally conducting but electrically insulating. This ensured that no short circuiting to the electrodes occurred. On the second sample of PMN–33PT, StyCast epoxy was used instead of GE varnish which is also thermally conducting but electrically insulating. Prior experiments established that there is little difference between the measurements made on samples mounted with either StyCast or GE varnish, but StyCast is mechanically stronger. Sample 1 was subsequently positioned on an alumina base, serving as a heat sink, and secured with GE varnish, while sample 2 was affixed using StyCast. A strain gauge was placed with GE varnish on sample 1 and with StyCast on sample 2 acting as the heater. Fig. S4a (ESI†) shows the mounting configuration of sample 1. The samples were then placed individually in a vacuumed environment inside a Lakeshore nitrogen-cooled cryostat. Sample 1 (labeled "fresh") was measured directly after mounting, while sample 2 (labeled "cycled") was cycled multiple times through its hysteresis loop at the various temperatures. The temperature was allowed to stabilize for at least one hour prior to each measurement. During both measurements, the electric field was maintained for about 5 minutes before the thermal conductivity was recorded to alleviate any pyroelectric artifacts.

The absolute value error of thermal conductivity near room temperature in the static heater and sink method is on the order of 10%. It is dominated by the radiative heat losses and by geometrical uncertainties. The latter is typically dominated by the distance between the thermocouples, where the error is given by the ratio between the size of the thermocouple contacts (which gives the uncertainty) and the distance between them. Here, this uncertainty is calculated to be 1.4–1.8%. In the cryostat, the radiative heat losses correspond to the thermal conductance that has been measured using a standard iron bar of known thermal conductivity; they are 0.10 mW K^{-1} at 200 K, 0.44 mW K^{-1} at 300 K and 0.85 mW K^{-1} at 360 K. Given the thermal conductivity and the geometry of the PMN–33PT samples, the losses represent $<7\%$ at 200 K, $<29\%$ at 300 K but $<55\%$ at 400 K. These losses have been subtracted from the measured conductance, but that procedure carries an uncertainty due to the difference in emissivity between the sample and the iron standard, which itself has an error of the order of 30%. Taken together, the radiative losses represent an uncertainty in the absolute values of 2% at 200 K, 10% at 300 K, but up to 18% at 360 K. The plots shown in Fig. 4 and Fig. S2 and S3 (ESI†) represent the field-dependence of the conductivity,

which is only affected by the relative error. This is much smaller and dominated by the noise on the thermocouples, equivalent to about 10 mK or 1% of the temperature difference and thus the measured conductivity.

Transverse piezoelectric coefficient d_{31}

To determine the d_{31} coefficient, we tracked the displacement of the top surface of the sample as a function of applied AC field. The sample measuring approximately 10 mm × 10 mm × 0.5 mm was securely affixed to a microscope glass slab using GE varnish. As the top surface was smaller than the laser beam size, a piece of Kapton tape was placed atop the sample. This layer provided a broader area for the laser beam to hit the edge of the sample ensuring a smaller measurement error by increasing the reflected signal. Fig. S4b (ESI†) shows the mounting configuration of the sample. For this displacement measurement, we relied on a Keyence LKG32 Laser Sensor. To apply the AC voltage, we employed a Techron 5050 Linear Amplifier in tandem with an Agilent 33120A Waveform Generator. Throughout the experiment, we continuously monitored the changes in the displacement using a Rigol MSO5074 oscilloscope.

A parallel experiment was carried out using the cycled sample. The objective of this second experiment was to elucidate the impact of cycling the sample through several sweeps of the electric field. The mounting of the sample for this experiment was slightly different from that of the first measurement. The laser beam hit the strain gauge placed on the top of the sample to measure the longitudinal displacement while applying the electric field. The d_{31} coefficient was calculated by taking the slope of the strain *vs.* electric field.

Longitudinal piezoelectric coefficient d_{33}

To measure the d_{33} coefficients, we used an MTI 2100 Fotonic measurement system while applying a DC voltage *via* a Stanford Research Systems' Data Precision 8200. The MTI 2100 Fotonic system utilizes fiber optics to precisely measure the small displacement parallel to the applied electric field. A fresh sample equipped with evaporated gold electrodes was placed inside a Poly K test fixture consisting of a metallic sample holder acting as an electrical conductor on the sample electrodes and a shiny metallic surface where the fiber optic light was reflected and output as a measured displacement. Both the sample holder and metallic surface are attached to micrometers allowing for precise positioning and instrument calibration. The fresh sample d_{33} coefficient was calculated by taking the slope of the strain *vs.* electric field and restricting the field to stay within the linear regime ($|E| \leq 2 \times 10^5$ V m^{-1}). The sample was then subjected to roughly 20 cycles of the electric field and the displacement tracked as a function of voltage. The d_{33} coefficient was calculated by taking the slope of the strain as a function of field. These measurements were repeated on three samples to test for reproducibility.

Results

The compound we used here was PMN–xPT ($0.3 \leq x \leq 0.33$) in single-crystal form. X-ray diffraction analysis showed a lattice constant of 4.026 Å at room temperature (see Fig. S1 in the ESI†). The material goes through several crystallographic phase transitions as a function of temperature and electric field.[12] At zero field, it is tetragonal (T) above about 320 K and monoclinic (M) below. The M phase contains two sub-phases, M_A and M_C, where the subscript denotes the different polarization vector directions. The phases are readily apparent in thermal conductivity measurements at zero field with the heat flux applied along the (100) direction, as shown in Fig. 1. Below ~225 K, PMN–33PT exists in the M_A phase, transitioning to the M_C phase between ~225 K and ~325 K. Beyond ~325 K, it adopts a T structure. Notably, as no electric field is applied at this time, the observed phase transitions solely occur because of temperature variations.

These phases are also dependent on the electric field. For example, if the sample is slightly above room temperature, it can transition from M_A to M_C with an increasing field. These transitions are obvious in the strain *vs.* electric field curves found in Davis *et al.*[12] Ultimately, these transitions are a function of the temperature, electric field, synthesis protocols, composition, and poling conditions.[12,13] For example, PMN–33PT has a large piezoelectric coefficient ~d_{33} = 1500 pC N^{-1};[14] a recent paper[13] related the poling conditions to d_{33} and found that d_{33} can change drastically with the poling electric field strength and AC or DC poling conditions. Tachibana *et al.*[4] reported a lower thermal conductivity for PMN-32PT, suggesting that thermal conductivity is highly sensitive to sample conditions and thermal stresses induced by cycling, including the growth method; a higher thermal conductivity is indicative of a more pristine sample. These materials are complex in structure that leads to a considerable spread in reported absolute values of κ.

The polarization *vs.* electric field along the (001) direction results at room temperature are shown in Fig. 2. The coercive

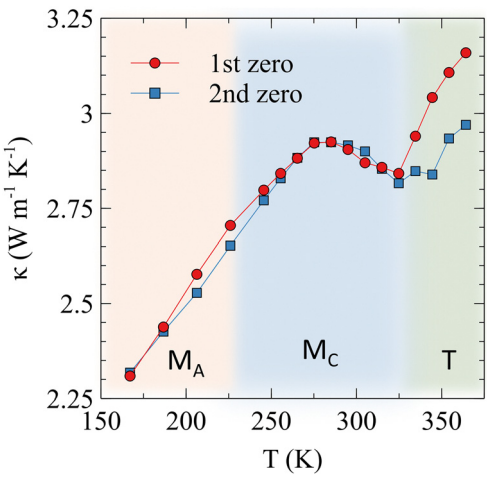

Fig. 1 Temperature dependent phase transitions observed in thermal conductivity measurements at zero field taken during field sweeps. In the legend, '1st zero' refers to the thermal conductivity value at zero field as the swept field is decreasing, and '2nd zero' refers to the value at zero field as the swept field is increasing (see later, Fig. 4). M_A, M_C, and T refer to the two monoclinic and tetragonal phases that PMN–33PT passes through as the temperature changes.

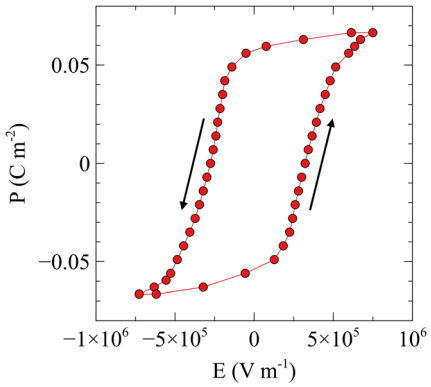

Fig. 2 Polarization of PMN–33PT at room temperature. Arrows indicate the direction of the swept field.

field is about 3×10^5 V m^{-1} and the saturation field is about 6×10^5 V m^{-1} with a polarization of about 0.06 C m^{-2}.

Fig. 3 shows the relative change with the electric field of the resonant frequency, f, that corresponds to the longitudinal compressive wave of the whole sample in the RUS. Because both f and the sound velocity of the LA phonon depend on the square root of the elastic constant c_{11}, this relative change equals the relative change in the sound velocity of the longitudinal acoustic phonon, *i.e.* $\frac{f - f_0}{f_0} = \frac{v'_{LA}}{v_{LA,0}}$. These measurements could not be taken on the cycled sample, as it had been instrumented for thermal conductivity measurements and its instrumentation perturbed the natural resonant frequencies of the sample.

Fig. 4a and b illustrate the behavior of the thermal conductivity of the fresh and cycled PMN–33PT samples with the field. The first run gives a $\frac{\kappa'}{\kappa_0}$ of almost 4×10^{-8} m V^{-1}. The

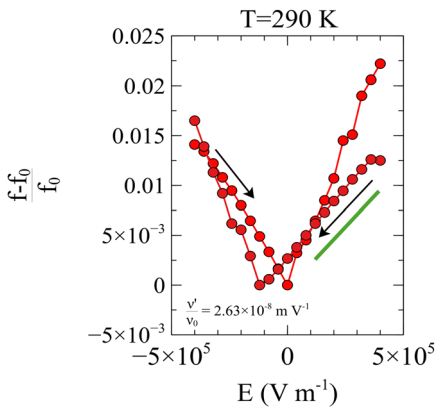

Fig. 3 Resonant ultrasound spectroscopy (RUS) measurement of the frequency of the resonance of the longitudinal compressive mode of a parallelepiped sample of PMN–33PT at 290 K. The relative change of this longitudinal resonant frequency is tracked as a function of electric field. This relative change of frequency equals the relative change of $\frac{v'}{v_0}$ of the longitudinal acoustic phonon along the (100) direction of the crystal. The green line indicates where the slope was taken to obtain the value of $\frac{v'}{v_0}$.

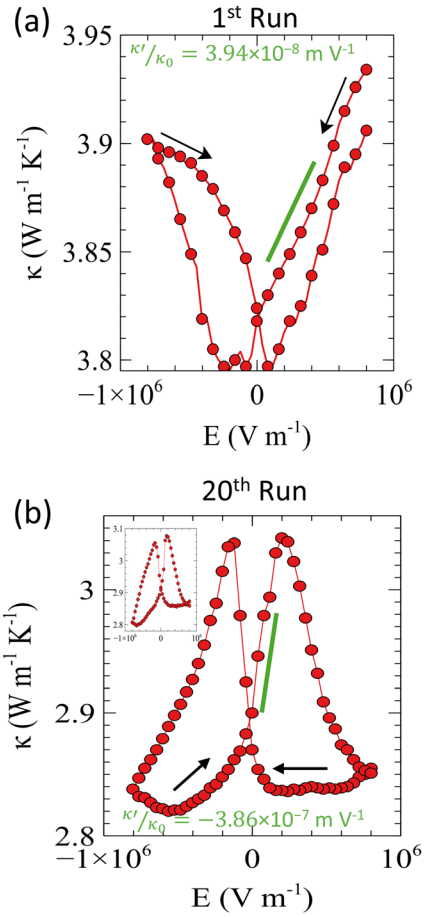

Fig. 4 (a) and (b) Room temperature thermal conductivity measurements on (a) a fresh sample on its first run and (b) a cycled sample on its 20th run. The (b) inset gives the data at the 10th run. This is essentially the same as at the 20th run, showing that while a transition occurs during the first 10 runs (see Fig. S2, ESI†), the sample is stable after about 10 cycles with electric field. The arrows indicate direction of sweep while the green line represents where the slope was taken to calculate the $\frac{\kappa'}{\kappa_0}$ values displayed below each plot.

thermal conductivity's field dependency changes during subsequent cycles of the positive and negative fields applied to the sample as shown in Fig. S2 (ESI†), which illustrates the first four cycles. The second sample cycled 20 times near room temperature (Fig. 4b) gives $\frac{\kappa'}{\kappa_0} = -3.86 \times 10^{-7}$ m V^{-1}. This condition is stable and reproducible (the curve after 10 cycles is shown in the inset and differs very little from the one cycled 20 times). The electric field dependence of the thermal conductivity shows a sign flip and is an order of magnitude larger *vis-à-vis* the fresh sample. The value is now two orders of magnitude larger than that reported in PZT $\left(\frac{\kappa'}{\kappa_0} = -7 \times 10^{-9} \text{ m V}^{-1}\right)$.[3] Considering the minimum and maximum thermal conductivity values, the change in the thermal conductivity of the cycled PMN–33PT sample with a field at room temperature is close to 8%. This increases to 11% at 364 K (see Fig. S3, ESI†).

Fig. 5 illustrates d_{31} measurements on two distinct samples: one pristine, untouched by an electric field, and the other, the

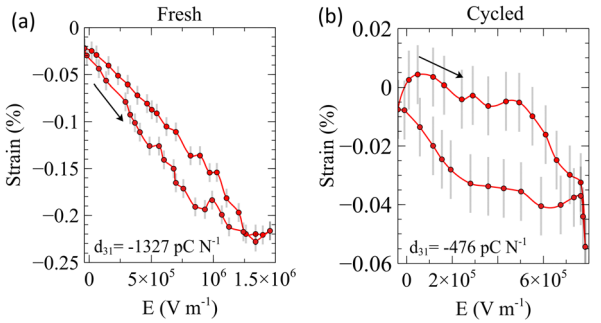

Fig. 5 (a) and (b) Transverse piezoelectric strain measurements on (a) a fresh PMN–33PT sample and (b) a cycled PMN–33PT sample. The slopes taken in decreasing field, indicated with arrows, were used to calculate the piezoelectric constant d_{31} values.

cycled sample previously employed for thermal conductivity measurements. To measure the transverse piezoelectric constant, we measured the change of the length of the sample along the (100) direction as a function of the electric field along the (001) direction. This change in the length of the sample corresponds to changes in the strain tensor; the derivative of these strain tensor components gives the piezoelectric coefficient.

We calculated a d_{31} of -1327 pC N^{-1} for the fresh sample and -476 pC N^{-1} for the cycled sample, a reduction of nearly three times.

We also investigated the longitudinal piezoelectric coefficient $-d_{33}$, corresponding to the displacement along the (001) direction parallel to the applied field. We measured d_{33} on a fresh sample by alternating between 0 and +100 V, back to zero to ensure that we remained in the linear regime and then to -100 V. This gave us a d_{33} of 1550 pC N^{-1} for the fresh PMN–33PT. We then cycled this sample roughly 20 times electrically. Fig. 6 shows the results for the cycled sample in which we obtained d_{33} = 2550 pC N^{-1} by averaging the slope in the positive and negative fields. Note that the zero-field value was zeroed out to account for hysteretic effects.

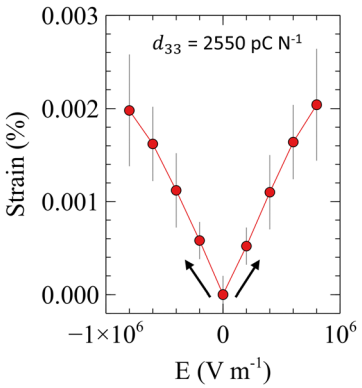

Fig. 6 Longitudinal piezoelectric measurement on a sample of PMN–33PT cycled ~20 times. The slope was averaged between the negative and positive fields to obtain a d_{33} value of 2550 pC N^{-1} for the cycled sample.

Discussion

Table 1 summarizes the values for d_{33}, d_{31}, $\frac{v'}{v_0}$ and $\frac{\kappa'}{\kappa_0}$, to be tested against eqn (3) and (4), with a Grüneisen parameter γ = 15 for PZT;[15] the same value will be assumed here for PMN–PT since $PbTiO_3$ is presumably the active ingredient. The measured d_{31} from Fig. 5a and d_{33} measured in the linear regime can be used to calculate the predicted values of $\frac{v'}{v_0}$ and $\frac{\kappa'}{\kappa_0}$ which correspond to the fresh sample depicted in Fig. 3 and 4a. The results, in the column labeled "Predicted" in Table 1, are quite close to the experimental values without the use of any adjustable parameter. Furthermore, eqn (4) holds approximately for the fresh sample, corroborating the hypothesis that τ has little field dependence. The initial results on fresh PMN–33PT are quantitatively explained by eqn (3) and (4) without adjustable parameters, just as the case for PZT.[3] Comparing the sound velocity and thermal conductivity results from Fig. 3 and 4a to that of PZT, we do indeed see the resulting curves of the PMN–33PT invert, and that the latter are an order of magnitude larger. The summation of the piezoelectric coefficients (d_{33} + $2d_{31}$) of PMN–33PT has the opposite sign than that of PZT,[3] leading to the sign inversion in the sensitivity of the sound velocity and thermal conductivity to the field. This adds definitive support to the theory[3,16] that the dispersion of acoustic phonons is affected by an external electric field and further, that acoustic phonons can thus be considered as ferrons carrying polarization, since at finite values for the phonon momentum they are coupled by piezoelectric strain to the optical phonons.

This treatment can be extended to the stable trace reported on the cycled sample in Fig. 4b, using the d_{31} value of -476 pC N^{-1} calculated from the measurement shown in Fig. 5b and the d_{33} value of 2550 pC N^{-1}. We were unfortunately unable to measure $\frac{v'}{v_0}$ on the cycled sample, as we prioritized the thermal conductivity measurements. The sample shattered into pieces too small for sound velocity measurements during dismount. The sign inversion between the cycled (Fig. 4b) and non-cycled (Fig. 4a) PMN–33PT is also predicted by the change in piezoelectric coefficients but not the additional increase in sensitivity by an order of magnitude.

We attribute this order of magnitude discrepancy between the predicted and measured $\frac{\kappa'}{\kappa_0}$ to the dependence of τ on the electric field (eqn (5)) observed in PMN-30PT.[2] A detailed study of the effect of scattering on the thermal conductivity using phonon lifetimes from inelastic neutron scattering is left for future work, as it has the potential to further enhance $\frac{\kappa'}{\kappa_0}$ and reach more practical thermal switching ratios.

To be complete, we must consider competing theories. Negi *et al.*[13] argue that a change in the thermal conductivity in PMN–PT can come from domain wall scattering. In principle, there must be a contribution of this mechanism to the electric field

Table 1 Material type, properties, predicted and measured $\frac{v'}{v_0}$ and $\frac{\kappa'}{\kappa_0}$ values for PZT, fresh PMN–33PT, and cycled PMN–33PT. All predicted values were calculated with $\gamma = 15$[15]

				Predicted	Measured	
Material	Type	d_{33} [pC N^{-1}]	d_{31} [pC N^{-1}]	$-\gamma(d_{33} + 2d_{31})$ [m V^{-1}]	$\frac{v'}{v_0}$ [m V^{-1}]	$\frac{\kappa'}{\kappa_0}$ [m V^{-1}]
PZT	FE	435[17]	−100[18]	-3.5×10^{-9}[3]	-3.3×10^{-9}[3]	-3.3×10^{-9}[3]
PMN–33PT (fresh)	RFE	1350	−1327	2.0×10^{-8}	2.6×10^{-8}	3.9×10^{-8}
PMN–33PT (cycled)	RFE	2550	−476	-2.4×10^{-8}	—	-3.9×10^{-7}

dependence of κ, but we argue that the principal mechanism arises through a change in the sound velocity and phonon spectrum. The first reason for this argument is the RUS measurements shown in Fig. 3, where we show unequivocally that the sound velocity depends on the electric field; sound velocity is a property at thermodynamic equilibrium and not a transport property. The second reason is that the domain sizes in Negi's work are of the order of 1 μm, much larger than the average phonon mean free path. While domain wall scattering has been shown unequivocally to cause an electric field dependence on the thermal conductivity at cryogenic temperatures,[5] this effect vanishes as the temperature increases to values where the phonon thermal mean free path becomes much smaller than the domain wall size, typically above 20 K.

Conclusions

In summary, our study involved measuring the thermal conductivity and sound velocity of PMN–33PT on two samples, one fresh and one cycled. The fresh sample exhibited values consistent with theoretical predictions based on the ferron theory and specific piezoelectric coefficients. The cycled sample, subjected to a sweeping electric field 20 times, displayed a sign change in $\frac{\kappa'}{\kappa_0}$ compared to the results obtained in the fresh sample and an increase by an order of magnitude. This suggested alterations in piezoelectric coefficients, as well as a possible contribution of an electric field-dependent relaxation time, probably induced by a change in the optical phonon modes. This would result in a much larger phase space for scattering of the acoustic modes. Interestingly, the summation $(d_{33} + 2d_{31})$ exhibited differing signs and values between PZT and PMN–33PT, and then a second sign change between the electrically cycled and the fresh sample of PMN–33PT. The calculated $\frac{\kappa'}{\kappa_0}$ values using measured d_{31} and d_{33} aligned with the expected piezoelectric coefficient changes outlined in the literature.[13] Though a magnitude difference in the cycled sample may relate to using samples with different histories and suspected electric field dependent scattering, further investigation is necessary. Comparing PMN–33PT with Wooten *et al.*'s[3] findings for PZT indicates an increase in the field sensitivity of the thermal conductivity by one order of magnitude for the fresh PMN–33PT sample and two orders of magnitude for the cycled sample, suggesting promising applications despite the need for further signal enhancement in studies on thermal switches.

Author contributions

DR was responsible for data curation, formal analysis, investigation, and writing – original draft and review and editing. BLW was responsible for data curation, formal analysis, investigation, visualization, supervision, and writing – original draft and review and editing. JPH was responsible for conceptualization, funding acquisition, supervision, and writing – original draft and review and editing.

Data availability

All data are shown in the manuscript and the ESI.† The raw data files acquired from the instruments or noted by hand in laboratory books data are available in numerical form from the authors.

Conflicts of interest

There are no conflicts to declare.

Acknowledgements

The primary funding for this work (DR and JPH) is from the US National Science Foundation grant CBET 213 3718. BLW is supported by a US Department of Defense SMART fellowship. The authors thank the OSU Smart Materials and Structures Lab, specifically Marcelo Dapino who assisted in d_{31} measurements. The authors thank Prof. Patrick Woodward for the engaging discussion involving relaxor ferroelectric materials. Metallization was conducted at OSU's Nanotech West Lab; the authors thank the lab manager, Paul Steffan, for the detailed training and guidance. Lastly, the authors thank Mohamed Nawwar for his assistance with XRD analysis.

References

1 G. E. W. Bauer, P. Tang, R. Iguchi, J. Xiao, K. Shen, Z. Zhong, T. Yu, S. M. Rezende, J. P. Heremans and K. Uchida, Polarization transport in ferroelectrics, *Phys. Rev. Appl.*, 2023, **20**, 050501.

2 M. E. Manley, D. L. Abernathy, R. Sahul, D. E. Parshall, J. W. Lynn, A. D. Christianson, P. J. Stonaha, E. D. Specht and J. D. Budai, Giant electromechanical coupling of relaxor ferroelectrics controlled by polar nanoregion vibrations, *Sci. Adv.*, 2016, **2**, e1501814.

3 B. L. Wooten, R. Iguchi, P. Tang, J. S. Kang, K.-I. Uchida, G. E. W. Bauer and J. P. Heremans, Electric field-dependent phonon spectrum and heat conduction in ferroelectrics, *Sci. Adv.*, 2023, **9**, eadd7194.
4 M. Tachibana and E. Takayama-Muromachi, Thermal conductivity and heat capacity of the relaxor ferroelectric $[PbMg_{1/3}Nb_{2/3}O_3]_{1-x}[PbTiO_3]_x$, *Phys. Rev. B: Condens. Matter Mater. Phys.*, 2009, **79**, 100104R.
5 A. J. H. Mante and J. Volger, Phonon transport in Barium Titanate, *Phys.*, 1971, **52**, 577–604.
6 G. Wehmeyer, T. Yabuki, C. Monachon, J. Wu and C. Dames, Thermal diodes, regulators, and switches: Physical mechanisms and potential applications, *Appl. Phys. Rev.*, 2017, **4**, 041304.
7 C. Liu, C. Wu, Y. Zhao, Z. Chen, T. L. Ren, Y. Chen and G. Zhang, Actively and reversibly controlling thermal conductivity in solid materials, *Phys. Rep.*, 2024, **1–32**, 1058.
8 J. F. Ihlefeld, B. M. Foley, D. A. Scrymgeour, J. R. Michael, B. B. McKenzie, D. L. Medlin, M. Wallace, S. Trolier-McKinstry and P. E. Hopkins, Room-temperature voltage tunable phonon thermal conductivity via reconfigurable interfaces in ferroelectric thin films, *Nano Lett.*, 2015, **15**(3), 1791–1795.
9 J. A. Seijas-Bellido, H. Aramberri, J. Íñiguez and R. Rurali, Electric control of the heat flux through electrophononic effects, *Phys. Rev. B*, 2018, **97**, 184306.
10 P. Torres, J. A. Seijas-Bellido, C. Escorihuela-Sayalero, J. Íñiguez and R. Rurali, Theoretical investigation of lattice thermal conductivity and electrophononic effects in SrTiO3, *Phys. Rev. Mater.*, 2019, **3**, 044404.
11 P. Torres, J. Íñiguez and R. Rurali, Giant Electrophononic Response in PbTiO3 by Strain Engineering, *Phys. Rev. Lett.*, 2019, **123**, 185901.
12 M. Davis, D. Damjanovic and N. Setter, Electric-field-, temperature-, and stress-induced phase transitions in relaxor ferroelectric single crystals, *Phys. Rev. B*, 2006, **73**, 014115.
13 A. Negi, H. P. Kim, Z. Hua, A. Timofeeva, X. Zhang, Y. Zhu, K. Peters, D. Kumah, X. Jiang and J. Liu, Ferroelectric Domain Wall Engineering Enables Thermal Modulation in PMN–PT Single Crystals, *Adv. Mater.*, 2023, **35**, 2211286.
14 T. Rojac, Piezoelectric response of disordered lead-based relaxor ferroelectrics, *Commun. Mater.*, 2023, **4**(1), 12.
15 Y. Fu and D. J. Singh, Thermal conductivity of perovskite KTaO3 and PbTiO3 from first principles, *Phys. Rev. Mater.*, 2018, **2**(9), 094408.
16 G. E. W. Bauer, R. Iguchi and K. Uchida, Theory of Transport in Ferroelectric Capacitors, *Phys. Rev. Lett.*, 2021, **126**, 187603.
17 Piezo-material-properties-data-sheet-20201112, (n.d.).
18 I. Kanno, S. Fujii, T. Kamada and R. Takayama, Piezoelectric properties of c-axis oriented Pb(Zr,Ti)O3 thin films, *Appl. Phys. Lett.*, 1997, **70**(11), 1378–1380.

